Supporting Information for "Hemoglobin Dynamics in Solution vis – à – vis Under Confinement – An Electrochemical Perspective"

*Rudra N. Samajdar[a], Gitanjali Asampille[b], Hanudatta S. Atreya[b], Aninda J. Bhattacharyya[a,]**

[a] Solid State and Structural Chemistry Unit, Indian Institute of Science, Bangalore: 560012, INDIA

[b] NMR Research Center, Indian Institute of Science, Bangalore: 560012, INDIA

*Corresponding author: anindajb@iisc.ac.in

CONTENTS

Title **Page No.**

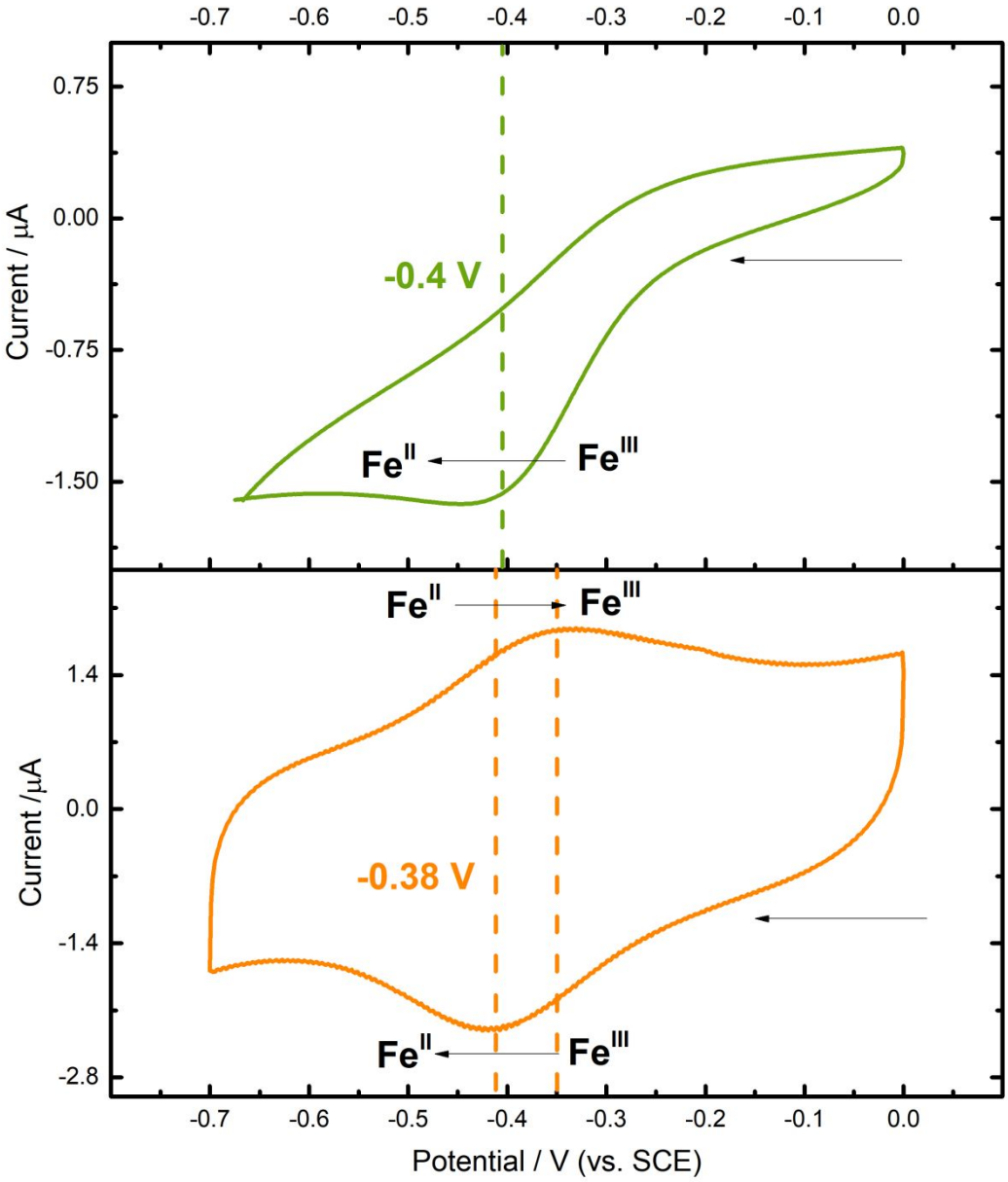

Figure S1: Cyclic voltammogram of hemoglobin in solution (top) and hemoglobin confined inside SiO_2 nanotubes of 200 nm diameter (scan rate 50mV/s). The arrows show the direction of potential scan and the redox processes corresponding to each peak are marked. Native hemoglobin in solution shows a distinct Fe (III) to Fe (II) transition, but the reverse process is not facile. Hemoglobin under confinement shows comparatively more facile redox. Further details about the electrochemistry has been reported from our group extensively earlier.[1-4] We

perform the experiments reported in this paper primarily to understand the reason for this unique electrochemical behaviour under confinement.

S1. Elastic Incoherent Neutron Scattering: Theory and Analysis

Neutron scattering accesses a wide range of timescales, characteristic of different dynamical modes of proteins and polymers (10 fs to 100 ns) and a corresponding wide variety of length scales (0.1 – 100 nm).[5] Incoherent elastic neutron scattering is used to sample collective motions across the polypeptide backbone of a protein spanning a range of 1 – 6 Å and 0.1 ns.[6]

In incoherent elastic neutron scattering experiments, the normalized incoherent elastic scattering function S (Q, ω=0) is studied as a function of temperature, where ω is the angular frequency and Q is the momentum transfer. Under the Gaussian approximation:[7]

$$\sqrt{\frac{\langle \Delta u^2 \rangle Q^2}{2}} \leq 1 \ldots\ldots\ldots (i)$$

Here $\langle u^2 \rangle$ is the root mean square displacement of the irreplaceable hydrogen atoms in the polymeric backbone. The elastic scattering intensity I (Q, ω=0) is given by:

$$I\,(Q,\omega = 0) = I_0 e^{-\frac{\langle \Delta u_{tot}^2 \rangle}{6} Q^2} \ldots\ldots\ldots (ii)$$

From a plot of I (Q, ω=0) versus Q^2, we extract the $\langle u^2_{tot} \rangle$ of the system. The temperature dependence of $\langle u^2_{tot} \rangle$ of the system is used to evaluate the "protein dynamics force constant":[8]

$$\langle k \rangle = \frac{0.00138}{\frac{d < 3u_{tot}^2 >}{dT}} \ldots\ldots\ldots (iii)$$

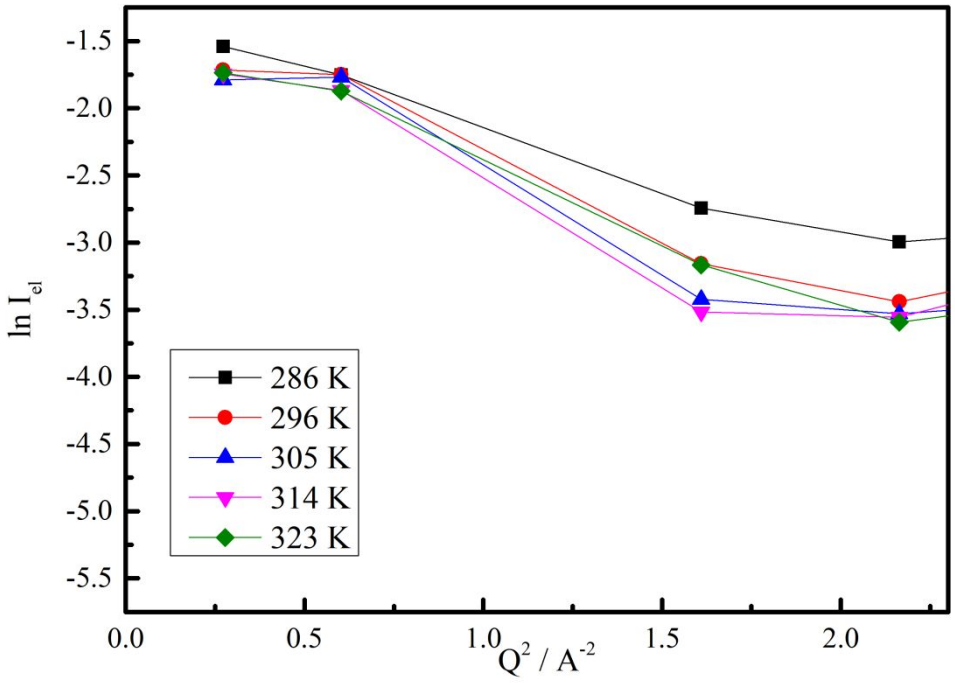

Figure S2: Variation of elastic incoherent scattering intensity of hemoglobin in solution (deuterated buffer, physiological pH 7.2) as a function of momentum transfer at the low q region ($Q^2 < 2$). The RMSDs of irreplaceable hydrogens along the protein backbone are extracted from this plot using the Gaussian approximation (discussed in detail in **Section S1**). The spectra are recorded under different temperature points as shown in the inset.

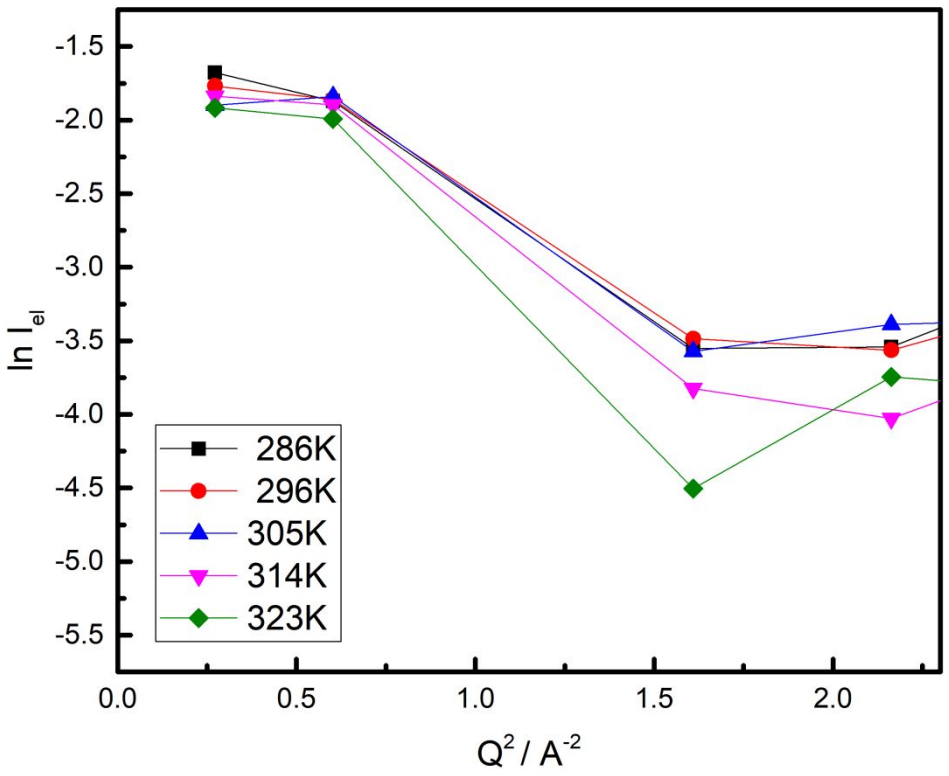

Figure S3: Variation of elastic incoherent scattering intensity of hemoglobin in silica nanotubes as a function of momentum transfer at the low Q regime ($Q^2 < 2$). The RMSD values of protons along the protein backbone are extracted from this data using the Gaussian model. The data are recorded across five different points in the temperature window along which the protein is physiologically active.

S2. Quasi-Elastic Neutron Scattering: Theory and Analysis

In quasi-elastic neutron scattering experiments, information can be obtained in the window of 3.5 – 14.5 Å and 1 ns. The Q averaged incoherent quasi - elastic neutron scattering structure function $\langle S(Q,\omega)\rangle_Q$ can be written as[9]:

$$< S(Q,\omega) >_Q = < e^{\frac{< u^2 >}{6} Q^2} >_Q [A_0\delta(\omega) + (1 - A_0)L(\omega)]R(\omega) + C \ldots\ldots\ldots (iv)$$

Here A_0 is the Elastic Incoherent Structure Factor (EISF), L(ω) is the Lorentzian Quasi Elastic Component, R(ω) is the experimental resolution function, and C is a flat background term added to take in to account inelastic contributions to the QENS energy region.

Further details can be obtained from the Q dependence of the function S(Q, ω):

$$< S(Q,\omega) >=< e^{\frac{< u^2 >}{6} Q^2} > [A_0(Q)\delta(\omega) + (1 - A_0(Q))L(Q,\omega)]R(Q,\omega) + C(Q) \ldots (v)$$

The Q dependence of the Lorentzian broadening and the EISF gives us more information about the type of motions involved.

S3. Diffusion Ordered Spectroscopy (DOSY): Theory and Analysis

This is a form of pulsed field gradient NMR technique used for measuring translational diffusion of molecules.[10-12] In the presence of varying field gradient, a pulsed field gradient spin echo experiment (1D) is done to monitor the signal intensity decay. The diffusion coefficient is calculated from this decay profile. Mathematically the decay is expressed as:

$$A_g = A_0 e^{-\gamma^2 g^2 \delta^2 \left(\Delta - \frac{\delta}{3}\right) D} \ldots\ldots\ldots (vi)$$

Here A_g is the signal intensity in the presence of gradient, A_0 is the signal intensity in the absence of gradient, γ is the gyromagnetic ratio, g is the strength of the diffusion gradients, δ is the gradient pulse duration, and Δ is the diffusion delay. This expression was proposed in the seminar paper by Stejskal and Tanner.[13] In a typical DOSY experiment, the strength of the diffusion encoding gradient is changed and the decaying signal intensities are fit to this Stejskal-Tanner expression. In the final 2D DOSY spectrum, the signals are dispersed according to chemical shift in one dimension and diffusion coefficient in one dimension.

The pulse gradient required to establish the diffusion coefficient measurement is well established in the literature. The diffusion coefficient is measured directly from the experiment and the radius of hydration of the molecule (assumed to be spherical) may be calculated using the Stokes – Einstein relationship:

$$D = \frac{kT}{6\pi\eta r} \ldots\ldots\ldots (vii)$$

Here, D is the observed diffusion coefficient, k is the Boltzmann constant, T is the temperature, η is the viscosity of the medium, and r is the radius of the molecule undergoing diffusion.

The DOSY experiments reported in this paper are performed on a Bruker Avance III 800 MHz NMR spectrometer equipped with a triple resonance TXI cryogenic probe. The variable

gradient diffusion data are acquired using stebpgp1s191D pulse programs for 1D (one-dimensional) DOSY and a stimulated echo stebpgp1s19 pulse program for (pseudo) 2D (two-dimensional) DOSY spectra with Watergate solvent suppression. Gradient pulses are applied for 0.9 msec with a recovery time of 1 sec, and a diffusion delay of 220 msec. Each experiment is acquired with a spectral width of 10,000 Hz, and 2k complex points. The data are zero-filled to 8k complex points, and apodized with a sine-squared function. The baseline is corrected with two separate polynomial functions, 0.15 ppm upfield and 0.15 ppm downfield of the water peak. The 2D DOSY spectra are processed in the corresponding two dimensions, chemical shifts (δ, ppm) in X-axis and translational diffusion coefficients (D, m^2s^{-1}) in Y-axis, with the DOSY module provided with the Top-Spin software 3.2.

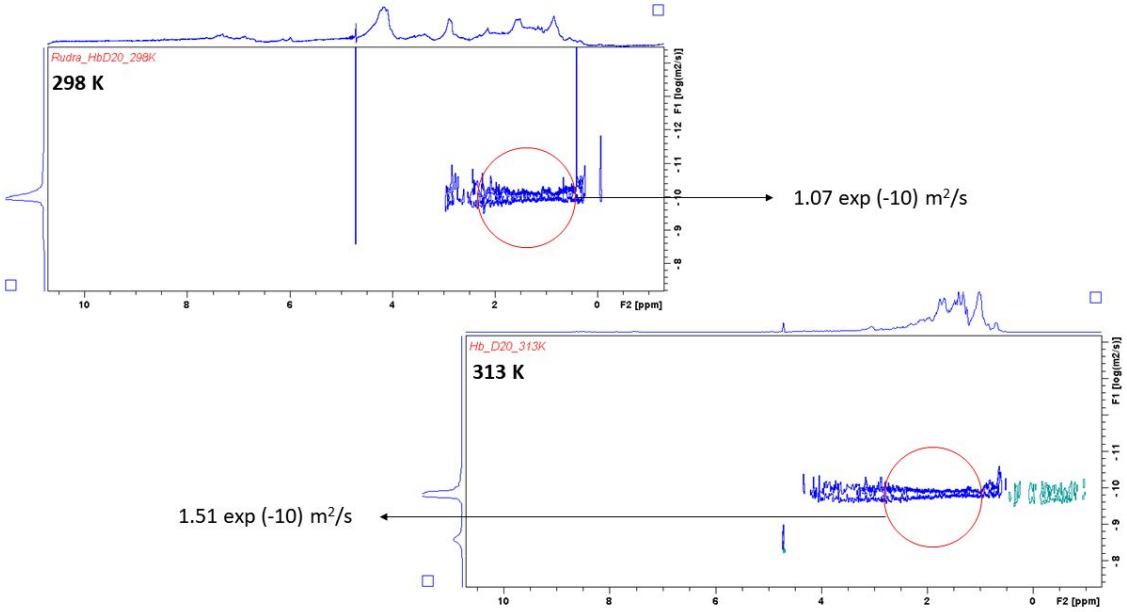

Figure S4: 2D Diffusion Ordered Spectroscopy (DOSY) spectra of hemoglobin in PBS buffer (pH 7.1). The spectra are recorded at two different temperatures (corresponding to those shown in the inset). Diffusion coefficients as obtained from the measurements are represented directly in the spectra as shown in red circles (see **Table 1**, main manuscript).

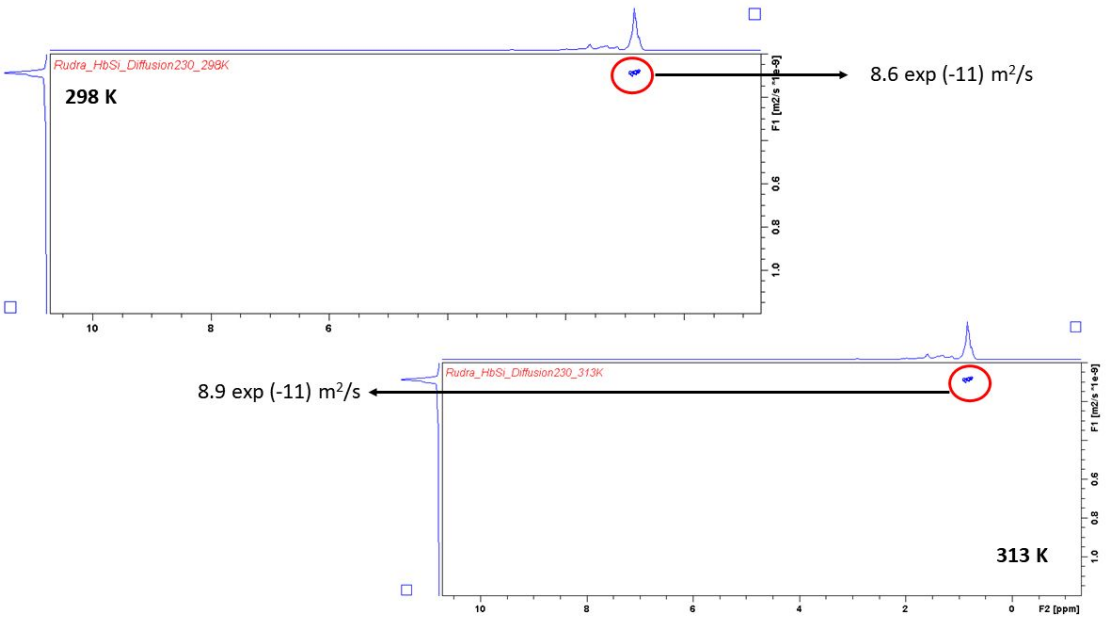

Figure S5: 2D Diffusion Ordered Spectroscopy (DOSY) of protein – silica matrix at 298 K and 313 K. The diffusion coefficients obtained are marked in red circles (see **Table 1**, main manuscript).

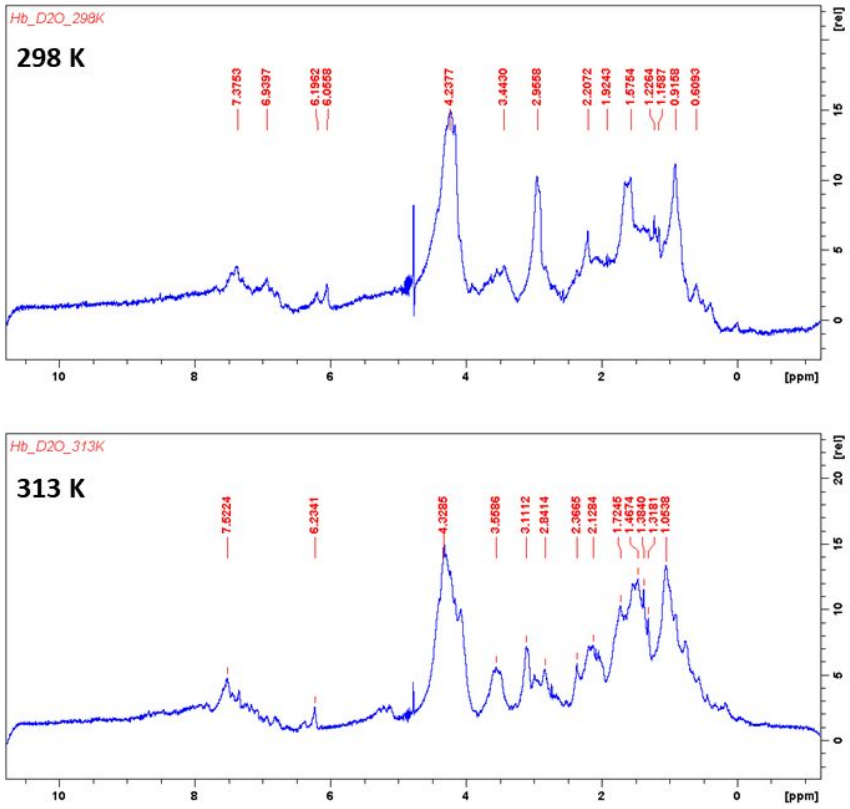

Figure S6: ^{1}H NMR spectra for hemoglobin in PBS buffer (pH 7.2) recorded at two different temperatures. Typical ^{1}H signals characteristic of the protein are marked in red. No significant change in the spectra indicate no denaturation of the protein at the temperature window used for performing the experiments.

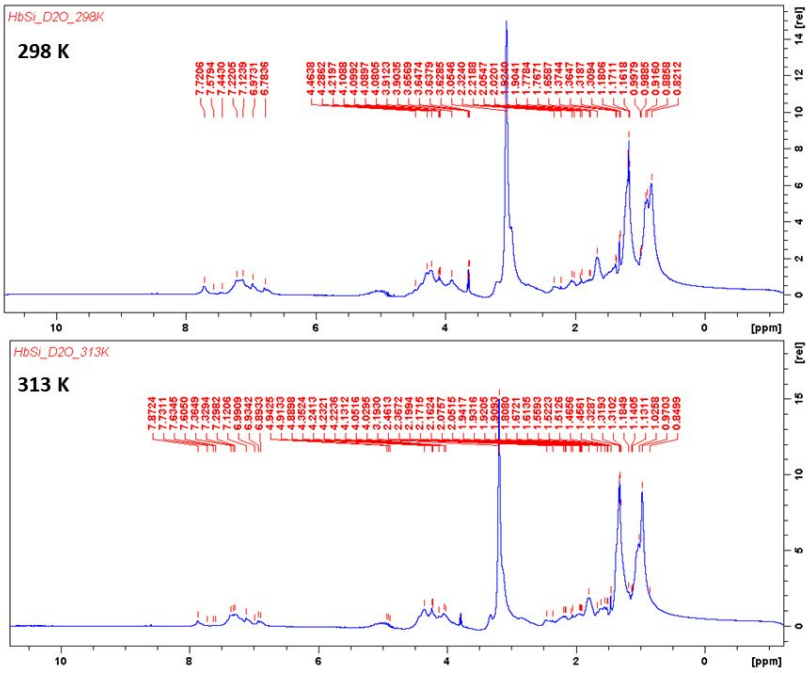

Figure S7: ^{1}H NMR of protein in silica matrix at two different temperatures (same as the temperatures used for protein in pH 7.2 solution). No significant change in spectra across the temperature range indicates stability of the protein – silica matrix complex in this temperature range.

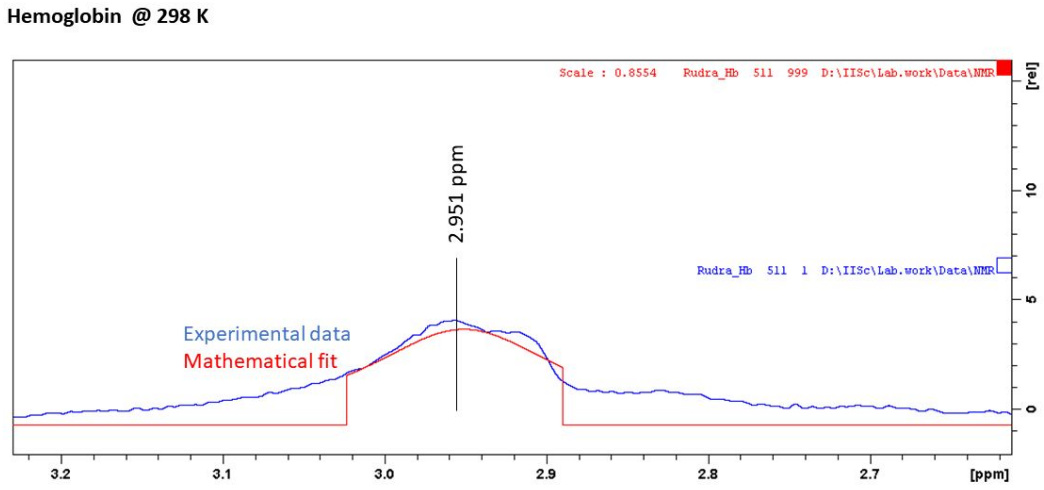

Figure S8: Typical lineshape fitting data for Hemoglobin at 298 K at pH 7.2 buffer. Shown here is the peak at 2.951 ppm fit using Voigt lineshape function using Bruker Topspin® 4.0.7 platform. The lineshape parameters are used to calculate the relaxation times reported in **Table 2**.

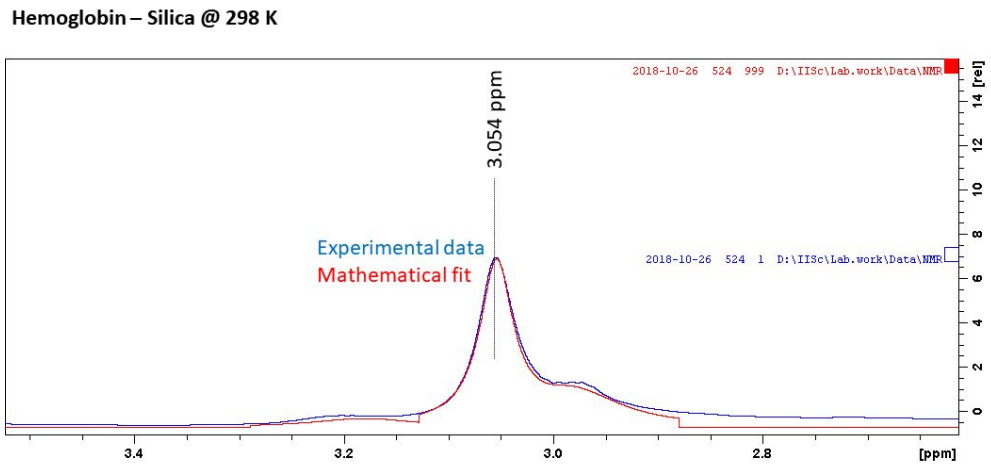

Figure S9: Typical linsehape fitting data for protein in silica matrix at 298 K. Shown here is the experimental and mathematically fit spectral line at 298K. The lineshape parameters are used to compute the relaxation times reported in **Table 2** in the main manuscript.

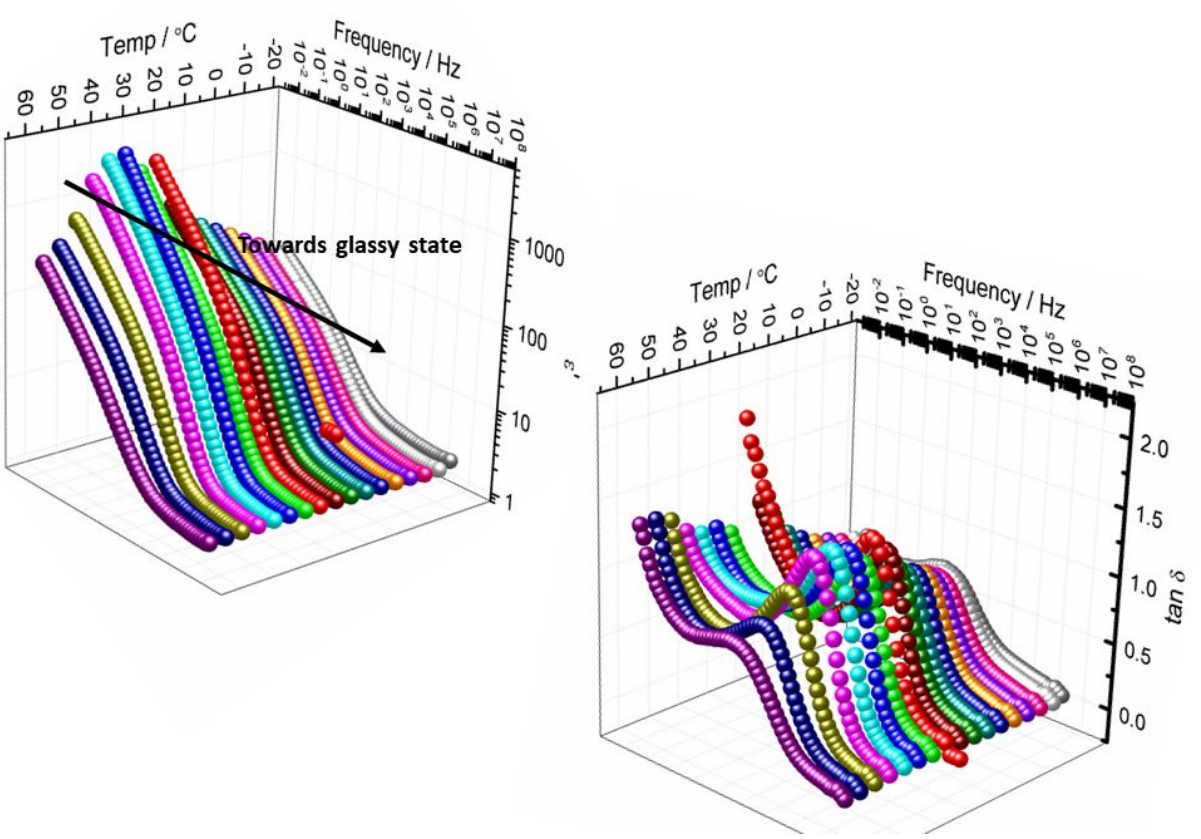

Figure S10: Temperature dependent dielectric relaxation spectra of hemoglobin confined in silica matrix. The top left panel depicts the frequency variation of the real part of the dielectric constant as a function of temperature, indicating an overall tendency of the system to move towards a glassy state at low temperatures. The lower right panel depicts the dielectric loss (tan δ) as a function of frequency and its variation with temperature. We note that the dielectric loss peak decreases in magnitude as we move from a native state of the protein to a glassy state at low temperatures. High temperatures also cause a decrease in the dielectric loss peak presumably due to denaturation/unfolding of the protein structure. All measurements are done on powdered samples to mitigate solvent conductivity effects.

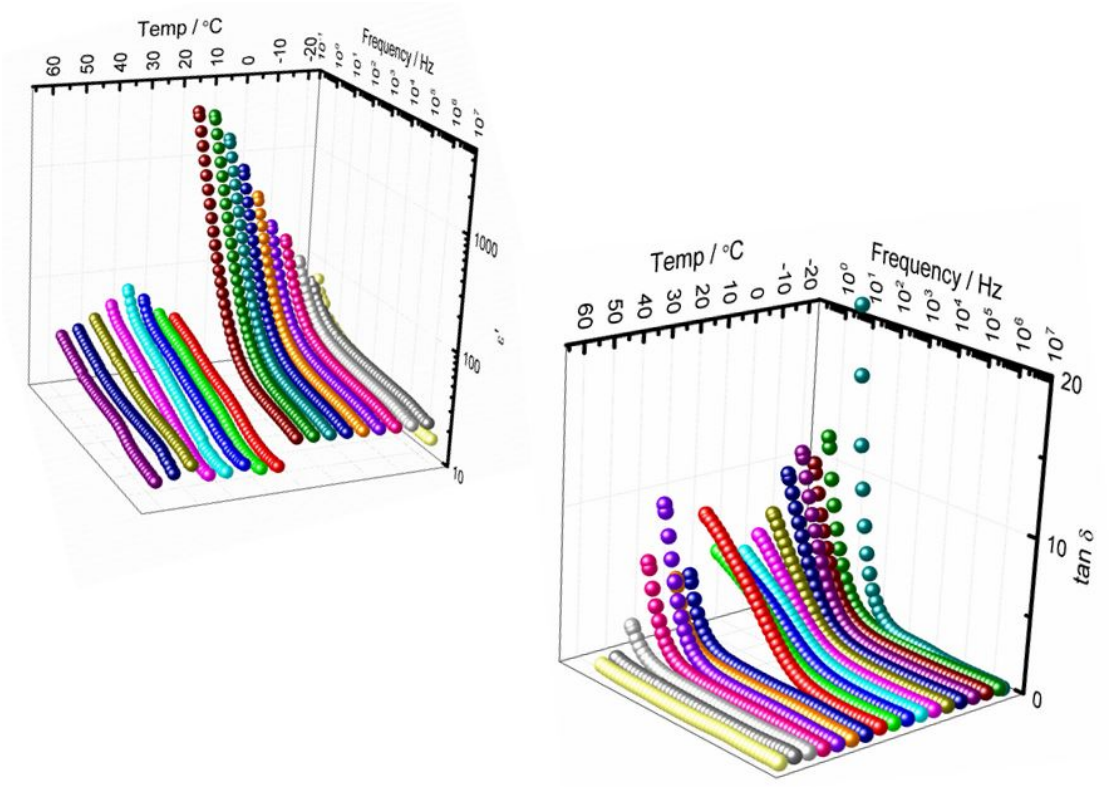

Figure S11: Dielectric relaxation spectra of non-confined (bulk) protein (in powdered form) as a function of temperature. The measurements are done in protein powder form (pellets recorded under parallel plate capacitor arrangement) as mentioned in **Figure S9** to mitigate solvent conductivity effects. The top left panel shows the real part of the dielectric constant as a function of frequency, and its variation with temperature. The bottom right panel shows the dielectric loss (tan δ) as a function of frequency and its variation with temperature. We note here that no distinct transitions are seen in the bulk protein powder over this temperature window indicating the presence of controlled hydration is essential for efficient dielectric response from the protein.

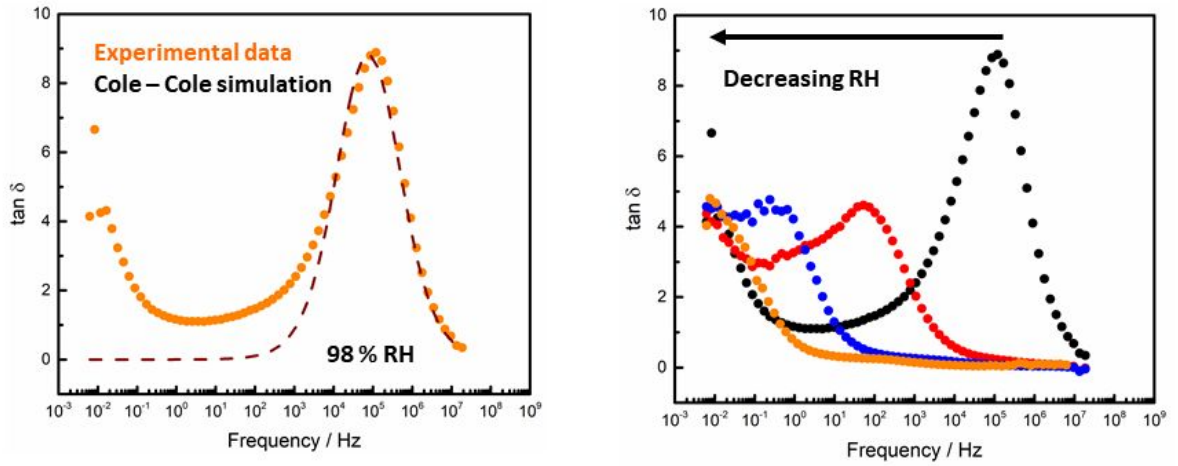

Figure S12: Dielectric relaxation spectra of hemoglobin in bulk powder as a function of hydration – experimental data, and Cole-Cole fit (discussed in detail in Section. The increase in tan δ at the low frequency limit is due to DC conductivity effects. (Left panel): Dielectric loss peak of hemoglobin at 298 K and 98% hydration (relative humidity/RH). (Right panel): Dielectric loss peak of hemoglobin at 298 K at different hydration levels: 98 % RH (black), 78 % (red), 58 % (blue), and 18 % (orange). This set of data clearly establish the requirement of an essential solvation sheath (hydration layer) around the protein for efficient dielectric response.

Relative Humidity (%)	Relaxation Lifetime / s
98 %	10^{-4}
78%	10^{-2}
58%	10^{2}
38%	10^{2}
18%	10^{3}

Table S1: Variation of dielectric relaxation lifetime of bulk protein as a function of relative humidity. The relaxation lifetimes are obtained by fitting the dielectric loss peaks (tan δ) to a Cole-Cole model (detailed discussion in **Section S4**).

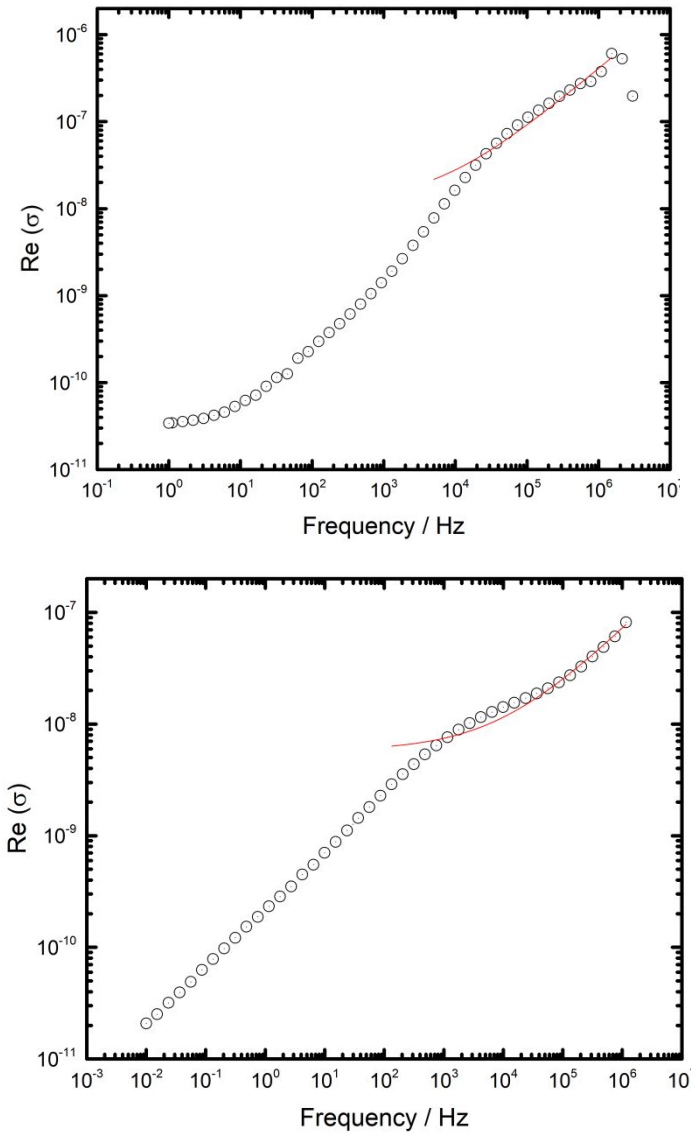

Figure S13: AC conductivity spectra of bulk hemoglobin (top) and hemoglobin:SiO_2 at 25°C. The data is fit to the universal dielectric response function: $\sigma = \sigma_{DC} + A\omega^s$ (discussed in the main text). The fit in the high frequency region is shown in red. Here σ represents the AC conductivity, A is a temperature dependent constant, ω is the AC frequency and s is an exponential factor lying between 0-1. The value of the σ_{DC} obtained from the fit (plateau region of the conductivity spectra) contributes to the dielectric constant at low frequencies.

S4. Dielectric Relaxation Spectroscopy: Theory and Analysis

In broadband dielectric relaxation spectroscopy, the complex dielectric constant of a material is measured over a wide range of AC frequencies, to delineate the effects of different types of polarization observed in the material.[14] Ideally, a material displays the following types of polarizabilities: electronic, atomic, dipolar, and space charge polarizability. These polarizabilities contribute to the dielectric response of the material under different frequency windows (**Figure S4.1**).

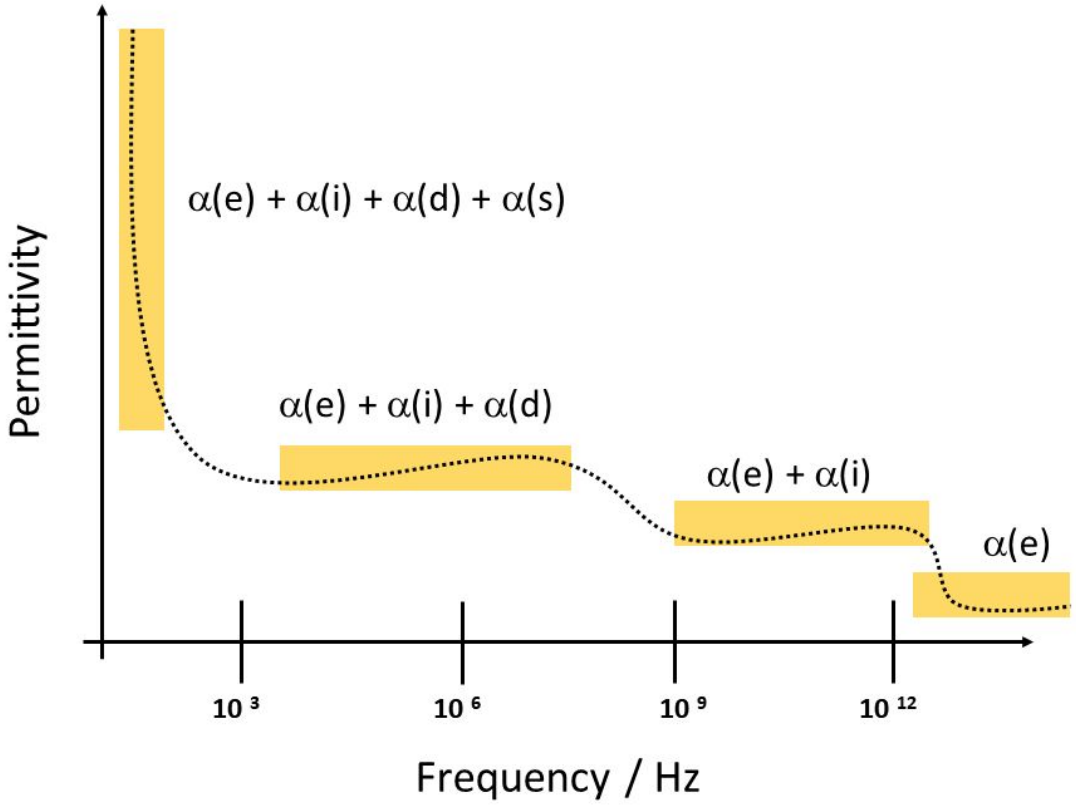

Figure S4.1: Typical dielectric relaxation spectrum across a broadband frequency range showing polarization effects α(e) – electronic, α(i) – ionic, α(d) – dipolar, and α(s) – space charge. The characteristic frequency ranges in which these effects are observed are marked in yellow panels.

The complex dielectric permittivity of a material is represented as:

$$\varepsilon^* = \varepsilon' - j\varepsilon''.....(viii)$$

Here,ε' and ε" are the real and complex parts of the dielectric permittivity respectively. There are various models used to understand the interaction among dipoles in a system. They differ in the mathematical analysis of the relaxation peak shape. The behavior of polar dielectrics at various frequencies is described by the Debye model[15]:

$$\varepsilon^* = \varepsilon_\infty + \frac{\varepsilon_s - \varepsilon_\infty}{1 + j\omega\tau}.....(ix)$$

Here ε_∞ and ε_s are high frequency and low frequency (space charge) values of the dielectric constant, ω is the angular frequency, and τ is the relaxation time.

In Cole-Cole model, a symmetric broadening of the Debye peak is observed:

$$\varepsilon^* = \varepsilon_\infty + \frac{\varepsilon_s - \varepsilon_\infty}{1 + (j\omega\tau_{C-C})^{1-\alpha}}.....(x)$$

The value of α lies between 0 and 1. $\tau_{c\text{-}c}$ is the mean relaxation time.

$$\varepsilon^* = \varepsilon_\infty + \frac{\varepsilon_s - \varepsilon_\infty}{1 + (j\omega\tau_{D-C})^{\beta}}.....(xi)$$

Here β lies between 0 and 1 and is a constant characteristic of the material, and $\tau_{D\text{-}C}$ is the mean relaxation time.

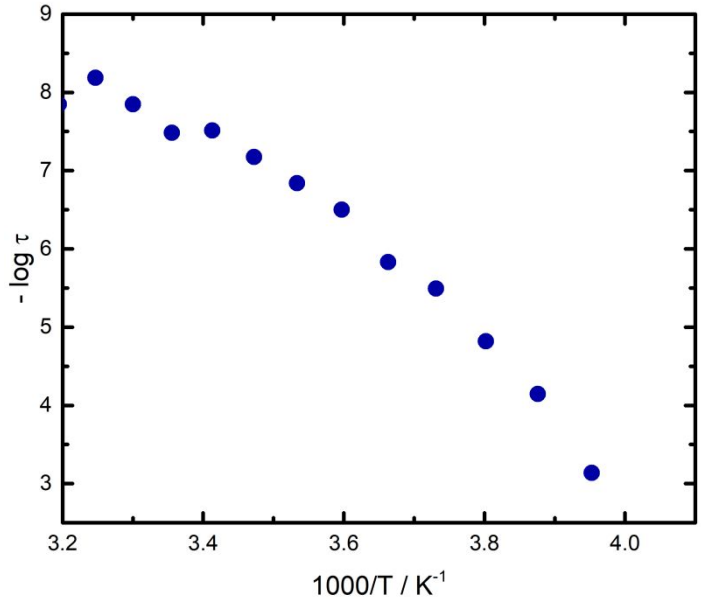

Figure S14: Temperature dependence of dielectric relaxation times obtained from confined hemoglobin. The systems show VTF behaviour over the temperature range shown here. Relaxation times are obtained after fitting to a Cole-Cole type of model along with DC conductivity corrections (Discussed in detail in **Section S4**, footnote of **Figure S13**, and the main text). The VTF parameters correspond to a glass transition temperature of 249°C, as compared to 220°C for the bulk sample.

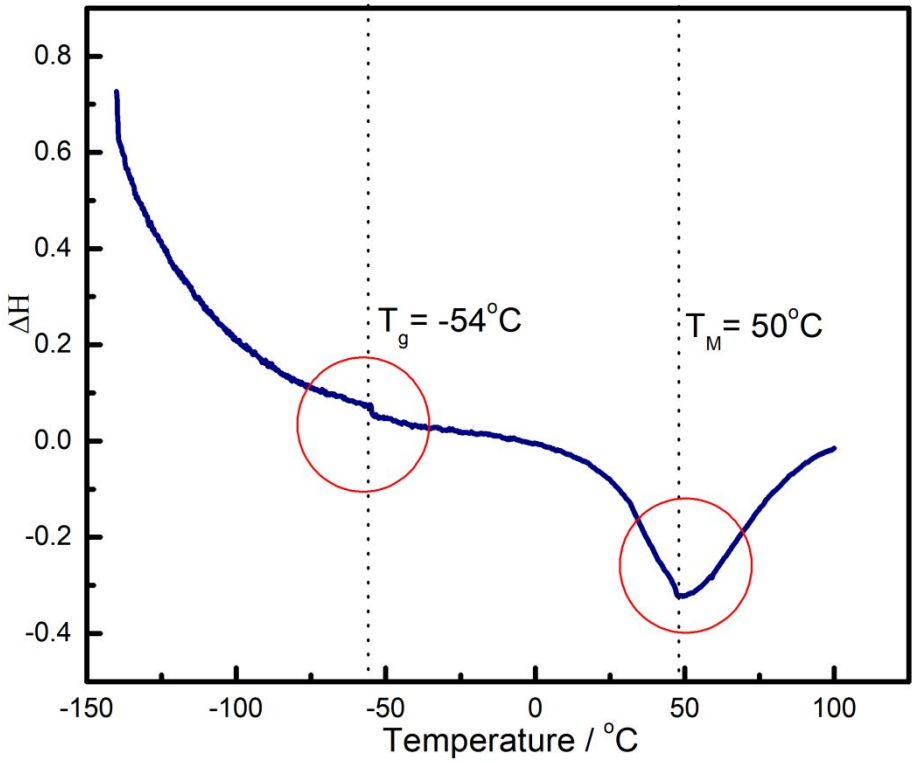

Figure S15: Typical DSC profile of bulk hemoglobin powder showing glass transition temperature (marked as T_g at -54°C) and folding-unfolding transition temperature (marked as T_M at 50°C). The glass transition temperature observed here corresponds to earlier reports in the literature on bulk hemoglobin.[16]

REFERENCES

1. Mandal, S. S.; Narayan, K. K.;Bhattacharyya, A. J. Employing Denaturation for Rapid Electrochemical Detection of Myoglobin Using Tio2 Nanotubes. *J. Mater. Chem. B* **2013**, *1*, 3051-3056.

2. Mandal, S. S.; Nagarajan, B.; Amenitsch, H.;Bhattacharyya, A. J. Probing Hemoglobin Confinement inside Submicron Silica Tubes Using Synchrotron Saxs and Electrochemical Response. *Eur. Biophys. J.* **2013**, *42*, 371-382.

3. Mandal, S. S.; Cristiglio, V.; Lindner, P.;Bhattacharyya, A. J. Small-Angle Neutron Scattering Studies of Hemoglobin Confined inside Silica Tubes of Varying Sizes. *ChemPhysChem* **2014**, *15*, 302-309.

4. Kapoor, S.; Mandal, S. S.;Bhattacharyya, A. J. Structure and Function of Hemoglobin Confined inside Silica Nanotubes. *J. Phys. Chem. B* **2009**, *113*, 14189-14195.

5. Jobic, H.;Theodorou, D. N. Quasi-Elastic Neutron Scattering and Molecular Dynamics Simulation as Complementary Techniques for Studying Diffusion in Zeolites. *Microporous Mesoporous Mater.* **2007**, *102*, 21-50.

6. Caronna, C.; Natali, F.;Cupane, A. Incoherent Elastic and Quasi-Elastic Neutron Scattering Investigation of Hemoglobin Dynamics. *Biophys. Chem.* **2005**, *116*, 219-225.

7. Becker, T.;Smith, J. C. Energy Resolution and Dynamical Heterogeneity Effects on Elastic Incoherent Neutron Scattering from Molecular Systems. *Physical Review E* **2003**, *67*, 021904.

8. Zaccai, G. How Soft Is a Protein? A Protein Dynamics Force Constant Measured by Neutron Scattering. *Science* **2000**, *288*, 1604-1607.

9. Bée, M. Quasielastic Neutron Scattering. **1988**.

10. Kerssebaum, R.;Salnikov, G., Dosy and Diffusion by Nmr. Bruker BioSpin GmbH, R., Germany, Ed. 2006.

11. Morris, K. F.;Johnson, C. S. Diffusion-Ordered Two-Dimensional Nuclear Magnetic Resonance Spectroscopy. *J. Am. Chem. Soc.* **1992**, *114*, 3139-3141.

12. Johnson Jr, C. S. Diffusion Ordered Nuclear Magnetic Resonance Spectroscopy: Principles and Applications. *Prog. Nucl. Magn. Reson. Spectrosc.* **1999**, *34*, 203-256.

13. Stejskal, E. O.;Tanner, J. E. Spin Diffusion Measurements: Spin Echoes in the Presence of a Time-Dependent Field Gradient. *J. Chem. Phys.* **1965**, *42*, 288-292.

14. West, A. R. *Solid State Chemistry and Its Applications*. John Wiley & Sons: 2014.

15. Raju, G. G. *Dielectrics in Electric Fields*. CRC press: 2017.

16. Liu, Z.; Huang, J.; Tyagi, M.; O'Neill, H.; Zhang, Q.; Mamontov, E.; Jain, N.; Wang, Y.; Zhang, J.;Smith, J. C. Dynamical Transition of Collective Motions in Dry Proteins. *Phys. Rev. Lett.* **2017**, *119*, 048101.